Check for updates

Sodium hydroxide and vacuum annealing modifications of the surface terminations of a Ti_3C_2 (MXene) epitaxial thin film†

Joseph Halim, [iD] * Ingemar Persson, [iD] Per Eklund, [iD] Per O. Å. Persson [iD] and Johanna Rosen

We investigate, and quantify, changes in structure and surface terminations of epitaxial thin films of titanium carbide (Ti_3C_2) MXene, when treated by sodium hydroxide solution followed by vacuum annealing at 550 °C. Using X-ray photoelectron spectroscopy and scanning transmission electron microscopy, we show that NaOH treatment produce an increase in the *c*-lattice parameter together with an increase in the O terminations and a decrease in the F terminations. There is also an increase in the percentage of the binding energy of Ti-species in Ti 2p XPS region, which suggests an increase in the overall oxidation state of Ti. After subsequent annealing, the *c*-lattice parameter is slightly reduced, the overall oxidation state of Ti is decreased, and the F surface terminations are further diminished, leaving a surface with predominantly O as the surface terminating species. It is important to note that NaOH treatment facilitates removal of F at lower annealing temperatures than previously reported, which in turn is important for the range of attainable properties.

Introduction

In 2011, a new family of 2D materials made of transition metal carbides and nitrides, so called MXenes, was discovered.[1] MXenes are produced from hexagonal layered transition metal carbides and nitrides known as MAX phases, described by the general formula $M_{n+1}AX_n$ (n = 1, 2, or 3), where M is a transition metal, A is an elements mainly from group 13–14 (Al, Ga, Si, or Ge) and X is C and/or N.[2] MXenes are synthesized by selective etching of the A layers (so far Al, Ga, and Si)[3–5] in the MAX phase, and replacing the etched atoms by a mixture of surface functional groups or surface terminations (T_x) of O, OH and/or F.[6] Thus, MXenes have a general formula of $M_{n+1}X_nT_x$. The etching can be done using various chemical compounds that contain fluoride ions and an acid. Among these compounds are HF, LiF and HCl, HF and LiCl, or NH_4HF_2.[6–9] MXenes have shown great promise for various applications,[10–12] including energy storage – Li-ion batteries[13] and supercapacitors[14] – hydrogen storage,[15] water purification,[16] electrochemical actuators,[17] photocatalysis,[18] catalysts for hydrogen evolution,[19] transparent conductive electrodes,[20] sensors,[21] thermoelectric materials,[22] and even phototherapy for cancer.[23]

The reduced dimensionality of 2D materials allow their properties to be significantly altered and affected by surface modifications, in particular through the introduction of surface terminations. As stated previously, MXenes have inherent surface terminations O, OH and/or F.[8] Several theoretical and experimental studies have dealt with identifying, quantifying and locating the sites of those surface terminations.[1,8,24–35] Also, attempts have been made to modify the surface terminations and investigate how such modification can affect the performance of MXenes for various applications. Among the various methods of modifying the surface terminations are annealing in vacuum and alkalization. For example, several studies showed an enhancement in electrical conduction of $Ti_3C_2T_x$ multilayers and single flakes after vacuum annealing.[36,37] Persson *et al.* showed the desorption of F terminations from $Ti_3C_2T_x$ multilayers when heating in vacuum above 600 °C using a combination of *in situ* heating in a scanning transmission electron microscope, STEM and X-ray photoelectron spectroscopy, XPS.[36] Dall'Agnese *et al.* reported the enhancement in capacitance for $Ti_3C_2T_x$ multilayers in H_2SO_4 after treatment with KOH.[37] As an important inspiration to our work, it has also been shown that treating multilayered $Ti_3C_2T_x$ powders with NaOH followed by vacuum annealing leads to an increase in electrical conductivity.[38] This was suggested to be due to the modification of the surface terminations, but without determination and quantification thereof. Overall, there has been little attention paid to identification and quantification of the modifications in the surface terminations as a result of treating the MXenes with alkali compounds followed by vacuum annealing. Very recently, Li *et al.* produced $Ti_3C_2T_x$ *via* alkali treatment for which T is only O and/or OH with no F. They

Thin Film Physics Division, Department of Physics, Chemistry and Biology (IFM), Linköping University, SE-58183 Linköping, Sweden. E-mail: joseph.halim@liu.se

† Electronic supplementary information (ESI) available: Details for XPS analysis of C 1s, Na 1s and Al 2p regions. See DOI: 10.1039/c8ra07270a

showed that this material has a capacitance of 314 F g^{-1}, which is about 214% higher than F terminated $Ti_3C_2T_x$ evaluated in 1 M of H_2SO_4.[39] This was achieved by the removal of Al from Ti_3AlC_2 *via* an alkali-assisted hydrothermal method (27.5 M NaOH, 270 °C).

Here, we present a detailed study aiming to quantify the changes in surface terminations and structure *via* XPS and STEM, respectively, when $Ti_3C_2T_x$ epitaxial thin films are first etched by HF 10% conc. and exposed to a NaOH solution, followed by vacuum annealing. We specifically choose thin films since they are advantageous over powders through their smoother surface and higher phase purity, that enables more reliable XPS measurements. The etching process is also faster and cleaner. Room temperature electrical resistivity measurements were also performed after each step, to show how the change in surface terminations resulting from NaOH treatment and vacuum annealing affect the electrical resistivity of $Ti_3C_2T_x$ thin film.

Experimental details

Deposition of Ti_3AlC_2

The Ti_3AlC_2 thin film was deposited using DC magnetron sputtering in an ultrahigh vacuum system of base pressure of <10^{-9} Torr, as in ref. 29. Three elemental targets (Ti, Al and C with diameters 75, 50 and 75 mm, respectively) were used to deposit the thin film on Al_2O_3 *c*-axis oriented (0001) substrates with surface area of 10 × 10 mm^2 and thickness 0.5 cm (MTI Corp. CA, USA). Prior to deposition, the substrates were cleaned *via* ultra-sonication in an acetone bath, followed by an iso-propanol bath, each for 10 min, and then dried by blowing nitrogen, N_2, gas. The substrate was preheated in the deposition chamber at 750 °C for 1 h. To form the Ti_3AlC_2 thin film, first, the Ti and C targets were ignited at powers of 92 and 142 W, respectively, for 5 s at 750 °C in Ar gas (99.9999% purity) at a constant chamber pressure of 4.8 mbar, to form a TiC (111) incubation layer that is <5 nm thick. The Al target is then ignited, at a power of 26 W for 0.3 h, forming an epitaxial Ti_3AlC_2 thin film which is ≈44 nm thick. Previous studies have shown that TiC incubation layers promote the growth of epitaxial Ti_3AlC_2 and other Ti-based MAX phase films.[40,41]

Synthesis of $Ti_3C_2T_x$ (MXene) thin films

The $Ti_3C_2T_x$ thin film was produced by selectively etching the Al layers from a Ti_3AlC_2 thin film using a 20 ml solution of 10% conc. HF (Sigma Aldrich, Stockholm, Sweden) for 2.5 h. After etching, the sample was rinsed in deionized (DI) water, followed by ethanol, and dried by blowing N_2 gas. The resulting $Ti_3C_2T_x$ film was then immersed in a solution of 1 g of NaOH pellets (Sigma Aldrich, Stockholm, Sweden) dissolved in 20 ml of DI for 1.5 h. The film was subsequently removed from the solution, rinsed with DI water and ethanol, and lastly dried by blowing N gas. This film is henceforth denoted as MX-Na.

Vacuum annealing of the film was performed inside the deposition system, at a base pressure of <10^{-9} mbar. The sample was first annealed at 60 °C for 4 h to remove most of the water residue. The film was then heated to 550 °C for 1 h and were then cooling down overnight to room temperature. This film – henceforth referred to as MX-Na-A – was then transferred to the XPS chamber as rapidly as possible. The maximum exposure of the film to the atmosphere was thus <5 min.

XRD measurements

X-ray diffraction (XRD) of the thin films was performed using a powder diffractometer (X'Pert, PANalytical, Almelo, The Netherlands) with a θ–2θ continuous scan of a step size of 0.017° and a 40 s dwell time.

TEM characterization

TEM samples were prepared by cutting out (0.5 mm) × (2 mm) pieces of the bulk sample and polished down to 80 μm thickness using diamond abrasive paper. Thereafter the samples were glued to a Mo half-grid and further polished from one side to 20 μm thickness. After that they were inserted into a Zeiss Crossbeam 1540 Focused Ion Beam (FIB) operated at 30 kV with a Ga ion beam for final thinning. The surface was protected by a thin Pt layer after which small thin cross-section lamellas were sliced out. This method does not require a lift out procedure, which is preferred when annealing experiments are required (the weld may cause unwanted effects). The samples were inserted in a Gatan double tilt furnace heating holder and heat treatment was performed inside the TEM in high vacuum up to 450 °C for 1 h. Characterization was performed using the Linköping double corrected FEI Titan[3] 60-300, equipped with a high-brightness gun (XFEG), monochromator, a Super-X EDX detector, and Quantum ERS-GIF. High-resolution STEM images during *in situ* annealing were acquired at 300 kV with ~0.7 Å resolution.

XPS analysis

The XPS measurements were performed using the XPS instrument (Kratos AXIS Ultra^{DLD}, Manchester, U.K.) using mono-chromatic Al-K_α (1486.6 eV) radiation. The thin film sample was mounted and clamped on the sample holder *via* copper strip for grounding. The X-ray beam irradiated the surface of the sample at an angle of 45°, with respect to the surface and provided an X-ray spot size of 300 × 800 μm. The electron analyzer accepted the photoelectrons perpendicular to the surface of the sample with an acceptance angle of ±15°. Charge neutralization was performed using a co-axial, low energy (~0.1 eV) electron flood source to avoid shifts in the recorded binding energy (BE). The details regarding XPS measurements and peak fitting can be found in the ESI.†

Resistivity measurements

Room temperature sheet resistance was measured using a four-point probe instrument (Jandel, model RM3000, UK). Five sheet resistance measurements were made for each case, and the resistivities determined by multiplying with the film thickness.

Results and discussion

XRD patterns for (i) Ti_3AlC_2, (ii) $Ti_3C_2T_x$, (iii) MX-Na, and (iv) MX-Na-A thin films are shown in Fig. 1a. The (000l) peaks of Ti_3AlC_2 and sapphire are identical to those reported in ref. 29. After etching, the (0002) peak shifts to lower angle, resulting in an increase in the c-lattice parameter (c-LP) from 18.5 to 20.8 Å, due to the removal of Al layers, followed by an exfoliation of the titanium carbide layers terminated by surface termination groups of (O, OH and/or F), in addition to intercalation of water layers.[8,9] After NaOH treatment, the c-LP increases to 25.3 Å. This increase can be attributed to the intercalation of Na^+ cations with most probably a layer of water.[9] After annealing the c-LP deceases slightly to 24.2 Å due to Na^+ de-intercalation and changes in the surface termination groups as shown by the XPS analysis discussed below.

A corresponding structural investigation of the films was performed by STEM as shown in Fig. 1b–d presenting cross-section overview images of an as etched sample ($Ti_3C_2T_x$), a NaOH intercalated sample (MX-Na), and a subsequently vacuum annealed sample (MX-Na-A), respectively.

The c-lattice parameters were measured for each sample by Fast Fourier Transform (FFT) analysis over the entire thickness of the films. FFT spots corresponding to the 002 reciprocal lattice points of $Ti_3C_2T_x$ yields the c-lattice parameters for $Ti_3C_2T_x$, MX-Na and MX-Na-A of 20.7 ± 0.2 Å, 25.2 ± 0.2 Å, and 24.4 ± 0.2 Å, respectively in agreement with the XRD results. It can be observed that the layered structure of the $Ti_3C_2T_x$ thin film is straightened and looks more regular after annealing.

Chemical analysis of the films was done by XPS. Fig. 2a–c, show the XPS spectra for Ti 2p, O 1s, F 1s regions, respectively, for $Ti_3C_2T_x$, MX-Na and MX-Na-A, together with their peak-fits. The peak positions, FWHMs, area percentage of the peaks, and peak assignments obtained from the fits, are summarized in Tables S1–S3 in the ESI,† respectively. XPS spectra for C1s, Na 1s and Al 2p regions are shown in Fig. S1† and their peak fitting information can be found in Tables S4–S6.† Global elemental

atomic percentage obtained from XPS are presented in Table S7 in the ESI.†

The Ti 2p region was fit by the components listed in column 5 in Table S1.† These peaks are assigned MXene surface Ti bound O and/or OH [(OH or O)–Ti–C, (OH or O)–Ti^{+2}–C, and (OH or O)–Ti^{+3}–C] and MXene surface Ti bound F [C–Ti–F_x]. Additionally, the peaks labelled TiO_2 and $TiO_{2-x}F_x$ are assigned to Ti atoms belonging to surface oxides, oxyfluorides, and/or Ti adatoms on the MXene surface bonded to O atoms, in agreement with observations in ref. 8, 9, 30 and 42.

The Ti 2p region for $Ti_3C_2T_x$ comprises primarily species belonging to the Ti_3C_2 compound, that is ~90% of the Ti 2p region, while the remaining 10% can be attributed to TiO_2 surface oxides. After the NaOH process ($Ti_3C_2T_x$-Na), the Ti species associated with the $Ti_3C_2T_x$ compound were found to be ~60% of the Ti 2p region, and the remaining ~40% is attributed to TiO_2 and $TiO_{2-x}F_x$ oxides and oxyfluorides. However, after annealing, the Ti species belonging to $Ti_3C_2T_x$ have restored their initial contribution by ~90% to the Ti 2p region.

The initial ratio of fraction of the three oxidation states of Ti (Ti, Ti^{+2}, Ti^{+3}) is estimated to 1 : 0.85 : 1.4, while upon NaOH treatment the fractional ratio of the three oxidation states changes to 1 : 2.4 : 3.4. Finally, upon annealing, the ratios change to 1 : 0.34 : 0.5. This indicates that upon NaOH treatment, the Ti in the $Ti_3C_2T_x$ compound has moved to a higher total oxidation state, while upon annealing the overall oxidation state is reduced.

The O 1s region of $Ti_3C_2T_x$ (Fig. 2b, bottom curve) was fit by the corresponding components: C–Ti–$O(I)_x$, C–Ti–$O(II)_x$, C–Ti–$(OH)_x$, $Al(OF)_x$ and $H_2O_{ads.}$ which are listed in column 5 in Table S3.† The peaks labelled C–Ti–$O(I)_x$ and C–Ti–$O(II)_x$ were assigned to MXene bound O bridging two Ti sites and the fcc site (also labelled A site), respectively, in agreement with previous investigations.[36] The peaks labelled C–Ti–$(OH)_x$ and $H_2O_{ads.}$ were assigned to MXene bound OH terminations and water, respectively, in agreement with ref. 8 and 9. The remaining O 1s region belongs to the peak labelled "$Al(OF)_x$"
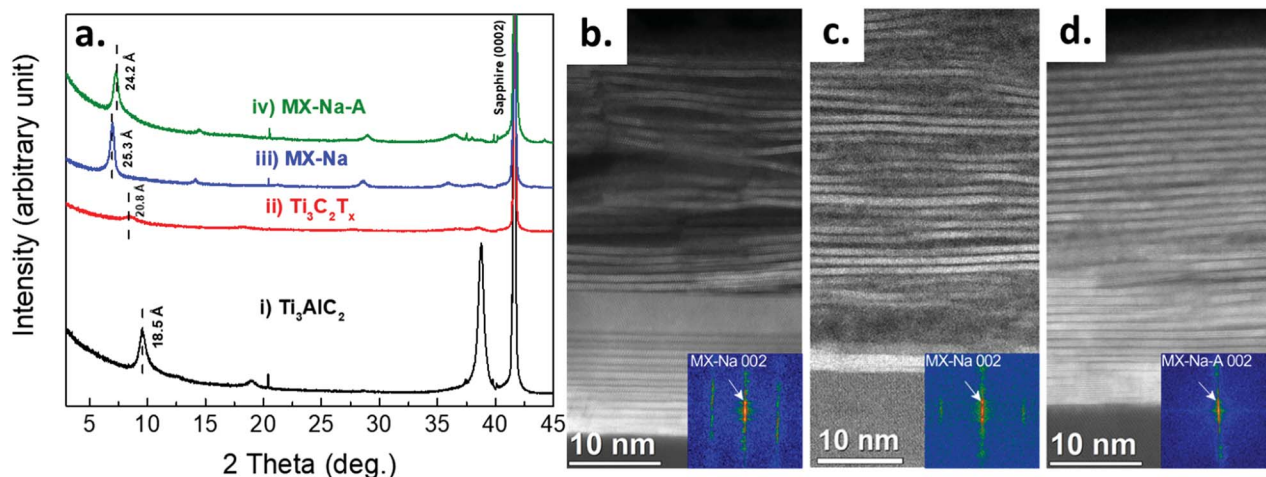

Fig. 1 (a) XRD patterns of (i) as-deposited Ti_3AlC_2 thin film, (ii) $Ti_3C_2T_x$, after etching in 10% HF for 2.5 h, (iii) MX-Na, after NaOH treatment, and MX-Na-A. Cross-sectional STEM overview images of (b) $Ti_3C_2T_x$, (c) MX-Na, and (d) MX-Na-A thin films. Insets show the corresponding FFTs. The 002 spots represent the c-lattice parameters of (b) 20.7 ± 0.2 Å, (c) 25.2 ± 0.2 Å, and (d) 24.4 ± 0.2 Å respectively.
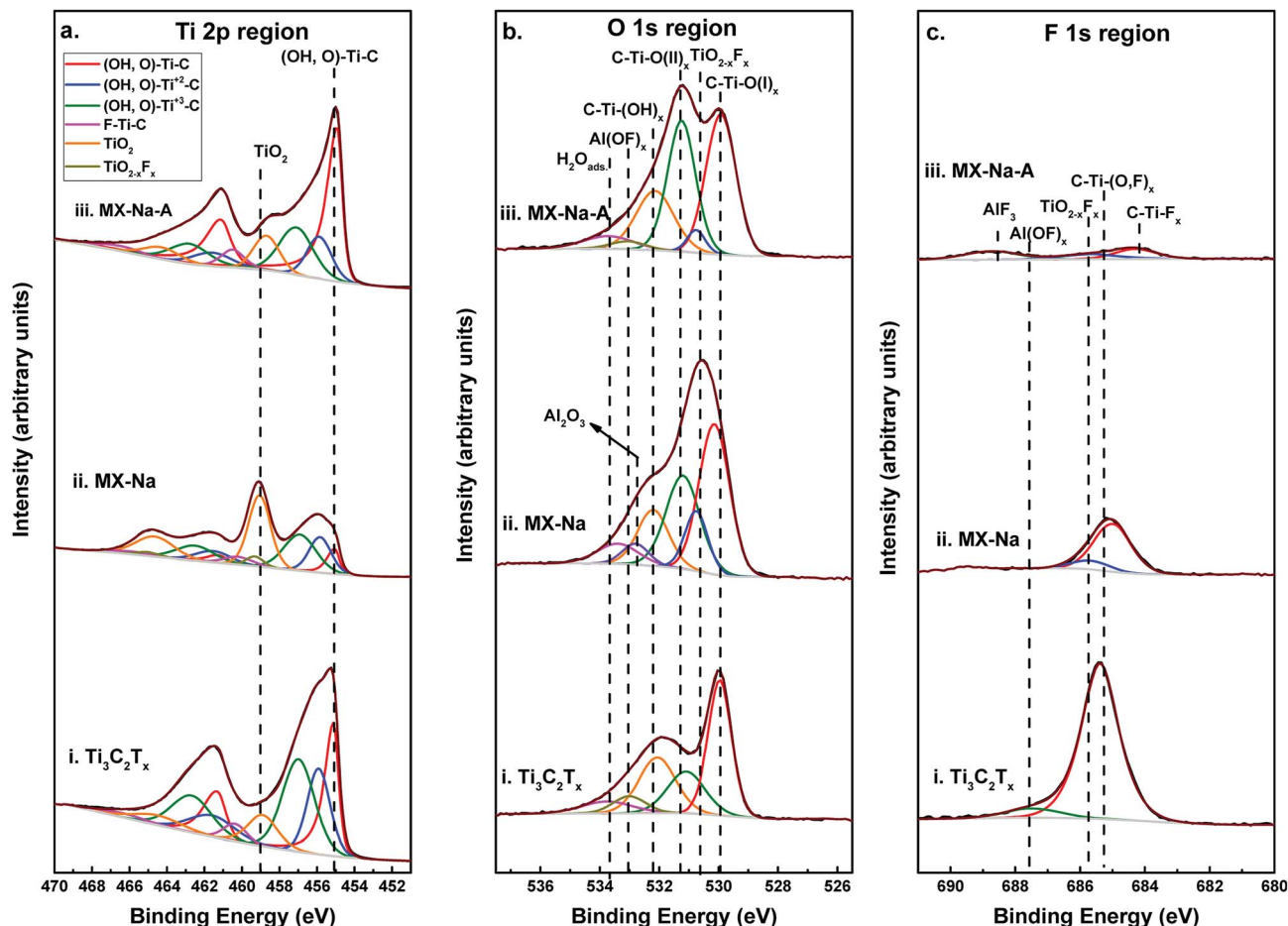
Fig. 2 XPS spectra with curve-fitting for (a) Ti 2p region for (i) $Ti_3C_2T_x$, (ii) MX-Na (iii) MX-Na-A. Dashed lines represent, from left to right, the species $F-Ti-C$ ($2p_{1/2}$), $TiO_{2-x}F_x$ ($2p_{1/2}$), TiO_2 ($2p_{1/2}$), (OH, O)$-Ti^{+3}-C$ ($2p_{1/2}$), (OH, O)$-Ti^{+2}-C$ ($2p_{1/2}$), (OH, O)$-Ti-C$ ($2p_{1/2}$), $F-Ti-C$ ($2p_{3/2}$), $TiO_{2-x}F_x$ ($2p_{3/2}$), TiO_2 ($2p_{3/2}$), (OH, O)$-Ti^{+3}-C$ ($2p_{3/2}$), (OH, O)$-Ti^{+2}-C$ ($2p_{3/2}$), and (OH, O)$-Ti-C$ ($2p_{3/2}$), respectively, these species are tabulated in Table S2.† (b) O 1s region for (i) $Ti_3C_2T_x$, (ii) MX-Na (iii) MX-Na-A. Dashed lines represent, from left to right, the species $H_2O_{ads.}$, $Al(OF)_x$, Al_2O_3, $C-Ti-(OH)_x$, $C-Ti-O(II)_x$, $TiO_{2-x}F_x$, and $C-Ti-O(I)_x$, respectively, these species are tabulated in Table S4.† (c) F 1s region for (i) $Ti_3C_2T_x$, (ii) MX-Na (iii) MX-Na-A. Dashed lines represent, from left to right, the species $C-Ti-O_x$, $TiO_{2-x}F_x$, $Al(OF)_x$, and AlF_3, respectively, these species are tabulated in Table S5.†

was assigned to O in aluminum oxyfluoride arising as a byproduct of the etching procedure.

The O 1s region of MX-Na (Fig. 2b, middle curve) was fit by the same components in addition to $TiO_{2-x}F_x$, belonging to surface oxyfluorides. After annealing, the percentage of MXene bound O [$C-Ti-O(II)_x$, $C-Ti-(OH)_x$, and $H_2O_{ads.}$] has increased from 47% of the O 1s region, before annealing, to 56% of the O 1s region as shown in Fig. 2b and Table S2 in the ESI.†

The F 1s region of $Ti_3C_2T_x$ (Fig. 2c lower curve) was fitted by two peaks of BEs 685.4 and 687.5 eV as shown in Table S4.† The first peak labelled "$C-Ti-(O,F)_x$" corresponds to F bonded to Ti, C and O atoms in $Ti_3C_2T_x$, as shown in ref. 36, and this peak occupies the majority of the F 1s region (97%). The second, close to negligible, peak labelled $Al(OF)_x$ corresponds to F species in Al oxyfluorides which are a byproduct of the etching process.[8]

After NaOH treatment, the intensity of the F 1s peak is significantly decreased (Fig. 2b, middle curve) and was fit by two species. The first and major one (∼85%) corresponds to $C-Ti-$

$(O,F)_x$ and the second one corresponds to titanium oxyfluoride resulting from oxidation. After vacuum annealing, the total intensity of the F 1s peak is almost vanished. The XPS spectrum was fit by three components labelled "$C-Ti-F_x$", "$TiO_{2-x}F_x$", and "AlF_3". The first peak which is 35% of the remaining F 1s region is assigned to F atoms bonded to Ti and C atoms in $Ti_3C_2T_x$, as shown in ref. 36. The other two peaks are assigned to titanium oxyfluoride and AlF_3, and they arise from surface oxidation and etching byproducts.

In order to investigate the changes in the chemistry of the $Ti_3C_2T_x$ thin films after NaOH treatment and vacuum annealing, the chemical formula of $Ti_3C_2T_x$ was calculated. The method of calculation and the assumptions used can be found in the ESI.†

As shown in Table 1 and Fig. 3, the chemical formula of the original $Ti_3C_2T_x$ MXene thin film is $Ti_3C_2O(I)_{0.2}O(II)_{0.3}$ $(OH)_{0.4}$-$F_{1.0} \cdot 0.1H_2O_{ads.}$. Here, the fluorine contributes to more than half of the surface termination species and the other half consists of O and OH. Upon the NaOH treatment, the number of moles of F

Table 1 Comparison of the chemical formula of $Ti_3C_2T_x$, $Ti_3C_2T_x$-Na, $Ti_3C_2T_x$-Na annealed thin films

$Ti_3C_2T_x$	$Ti_3C_2O(I)_{0.2}O(II)_{0.3}(OH)_{0.4}F_{1.0}$ $0.1H_2O_{ads.}$ Total sum of surface terminations is 1.9
MX-Na	$Ti_3C_2O(I)_{0.3}O(II)_{0.9}(OH)_{0.5}F_{0.6}$ $0.3H_2O_{ads.}$-0.7Na Total sum of surface terminations is 2.3
MX-Na-A	$Ti_3C_{1.8}O(I)_{0.3}O(II)_{1.0}(OH)_{0.4}F_{0.05}$ $0.2H_2O_{ads.}$-0.04Na Total sum of surface terminations is 1.75
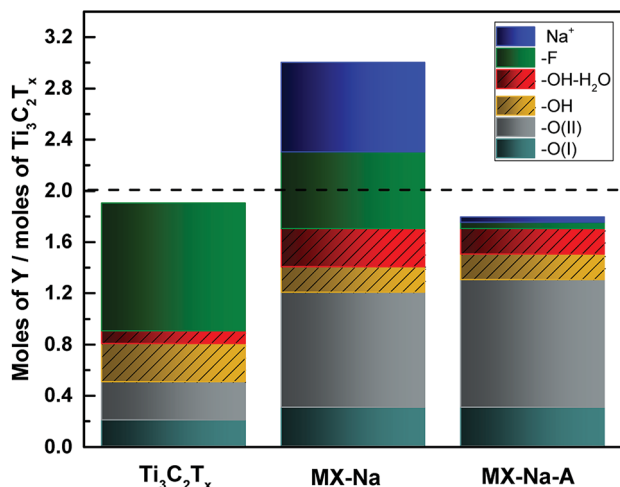
Fig. 3 Moles of Y per $Ti_3C_2T_x$ formula unit for $Ti_3C_2O(I)_{0.2}O(II)_{0.3}(OH)_{0.4}F_{1.0}$ $0.1H_2O_{ads.}$, $Ti_3C_2O(I)_{0.3}O(II)_{0.9}(OH)_{0.5}F_{0.6}$ $0.3H_2O_{ads.}$-0.7Na, and $Ti_3C_{1.8}O(I)_{0.3}O(II)_{1.0}(OH)_{0.4}F_{0.05}$ $0.2H_2O_{ads.}$-0.04Na. Y includes the surface terminations and adsorbed H_2O. Note that if one termination is assumed per surface M atom, then the theoretical T_x number per formula is 2 given by the horizontal dashed line.

surface termination group per mole of $Ti_3C_2T_x$ are reduced from 1.0 to 0.7 moles and the O and OH surface termination groups experience an increase from 0.5 to 1.2 and from 0.4 to 0.5 moles per mole of $Ti_3C_2T_x$, respectively, as shown in Fig. 3. After heat treatment, most of the F surface termination was removed, leaving only 0.05 moles of F. It is important to note that the significant reduction of –F after NaOH treatment and vacuum annealing, occurs at a much lower annealing temperature and for shorter duration of time than that reported in ref. 36 where vacuum annealing is performed without NaOH treatment. Hence, the F reduction is predominantly associated with the proceeding NaOH treatment. The majority of the surface termination becomes O, 1.3 moles per mole of $Ti_3C_2T_x$, and less than one third of that amount is the level of OH, 0.4 moles per mole of $Ti_3C_2T_x$. The increase in O surface terminations are associated with the increased O(II) peak observed by XPS. This can be understood from the additional O introduced in the preceding NaOH treatment, which move in to occupy the vacant (and preferred) sites left behind in the F desorption process.[36] A significant decrease in the intercalated Na^+ cations after vacuum annealing, from 0.7 to 0.04 moles per mole of $Ti_3C_2T_x$, was also observed.

The resistivity of the as-etched film was 12.6 ± 0.7 μΩ m. After treatment with NaOH, the resistivity increased to 41 ± 2 μΩ m. Annealing reduced the resistivity to 12.6 ± 1 μΩ m. In

other words, the resistivity of $Ti_3C_2T_x$ thin film increased 3 times after the NaOH treatment then returned back to its original value after annealing. These results confirm what has been reported by Wang et al.[38] Similar behavior has been reported by Römer et al.,[43] showing the oxidation and increase in resistivity of a free standing $Ti_3C_2T_x$ film after O plasma treatment followed by reduction and a decrease in the resistivity of the same film after hydrogen plasma treatment from 5.6 to 4.6 μΩ m.

Conclusion

Through XPS analysis we have investigated the change in surface terminations of an epitaxial thin film of $Ti_3C_2T_x$ MXene upon NaOH treatment followed by vacuum annealing at 550 °C for 1 h. Corresponding structural analysis was performed through XRD and TEM. Upon NaOH treatment, the surface terminations change from a more fluorinated surface termination to a more oxygenated surface termination, accompanied by an indication of an increase in the oxidation state for the Ti in the $Ti_3C_2T_x$ compound. After annealing, the total amount of surface terminations has decreased, and since primarily fluorine terminations are reduced, a majority of O surface terminations are present. Also, a decrease in the oxidation state of Ti is suggested due to the removal of the fluorine surface termination causing some of the Ti atoms to be unterminated. The results show that NaOH treatment facilitates a change towards an O-terminated surface at reduced annealing temperatures compared to previous studies. This is of importance for surface functionalization and property tuning. The resistivity of $Ti_3C_2T_x$ thin film was found to increase from 12.6 to 40.8 μΩ m after NaOH treatment, then decreases back to its original value after vacuum annealing. This is in line with the change in the surface chemistry and structure of $Ti_3C_2T_x$ upon alkali treatment and vacuum annealing.

Conflicts of interest

There are no conflicts to declare.

Acknowledgements

References

1 M. Naguib, M. Kurtoglu, V. Presser, J. Lu, J. Niu, M. Heon, L. Hultman, Y. Gogotsi and M. W. Barsoum, *Adv. Mater.*, 2011, **23**, 4248–4253.

2 M. W. Barsoum, *MAX Phases: Properties of Machinable Ternary Carbides and Nitrides*, John Wiley & Sons, 2013.

3 M. Naguib, M. Kurtoglu, V. Presser, J. Lu, J. J. Niu, M. Heon, L. Hultman, Y. Gogotsi and M. W. Barsoum, *Adv. Mater.*, 2011, **23**, 4248–4253.

4 J. Halim, S. Kota, M. R. Lukatskaya, M. Naguib, M. Q. Zhao, E. J. Moon, J. Pitock, J. Nanda, S. J. May, Y. Gogotsi and M. W. Barsoum, *Adv. Funct. Mater.*, 2016, **26**, 3118–3127.

5 M. Alhabeb, K. Maleski, T. S. Mathis, A. Sarycheva, C. B. Hatter, S. Uzun, A. Levitt and Y. Gogotsi, *Angew. Chem., Int. Ed.*, 2018, **57**, 5444–5448.

6 M. Naguib, O. Mashtalir, J. Carle, V. Presser, J. Lu, L. Hultman, Y. Gogotsi and M. W. Barsoum, *ACS Nano*, 2012, **6**, 1322–1331.

7 M. Ghidiu, M. R. Lukatskaya, M.-Q. Zhao, Y. Gogotsi and M. W. Barsoum, *Nature*, 2014, **516**, 78–81.

8 J. Halim, K. M. Cook, M. Naguib, P. Eklund, Y. Gogotsi, J. Rosen and M. W. Barsoum, *Appl. Surf. Sci.*, 2016, **362**, 406–417.

9 M. Ghidiu, J. Halim, S. Kota, D. Bish, Y. Gogotsi and M. W. Barsoum, *Chem. Mater.*, 2016, **28**, 3507–3514.

10 J.-C. Lei, X. Zhang and Z. Zhou, *Front. Phys.*, 2015, **10**, 276–286.

11 B. Anasori, M. R. Lukatskaya and Y. Gogotsi, *Nat. Rev. Mater.*, 2017, **2**, 16098.

12 P. Eklund, J. Rosen and P. O. Å. Persson, *J. Phys. D: Appl. Phys.*, 2017, **50**, 113001.

13 M. Naguib, J. Halim, J. Lu, K. M. Cook, L. Hultman, Y. Gogotsi and M. W. Barsoum, *J. Am. Chem. Soc.*, 2013, **135**, 15966–15969.

14 M. R. Lukatskaya, S. Kota, Z. Lin, M.-Q. Zhao, N. Shpigel, M. D. Levi, J. Halim, P.-L. Taberna, M. W. Barsoum, P. Simon and Y. Gogotsi, *Nat. Energy*, 2017, **2**, 17105.

15 Q. Hu, D. Sun, Q. Wu, H. Wang, L. Wang, B. Liu, A. Zhou and J. He, *J. Phys. Chem. A*, 2013, **117**, 14253–14260.

16 Q. Peng, J. Guo, Q. Zhang, J. Xiang, B. Liu, A. Zhou, R. Liu and Y. Tian, *J. Am. Chem. Soc.*, 2014, **136**, 4113–4116.

17 J. Come, J. M. Black, M. R. Lukatskaya, M. Naguib, M. Beidaghi, A. J. Rondinone, S. V. Kalinin, D. J. Wesolowski, Y. Gogotsi and N. Balke, *Nano Energy*, 2015, **17**, 27–35.

18 Z. Guo, J. Zhou, L. Zhu and Z. Sun, *J. Mater. Chem. A*, 2016, **4**, 11446–11452.

19 Z. W. Seh, K. D. Fredrickson, B. Anasori, J. Kibsgaard, A. L. Strickler, M. R. Lukatskaya, Y. Gogotsi, T. F. Jaramillo and A. Vojvodic, *ACS Energy Lett.*, 2016, **1**, 589–594.

20 K. Hantanasirisakul, M. Q. Zhao, P. Urbankowski, J. Halim, B. Anasori, S. Kota, C. E. Ren, M. W. Barsoum and Y. Gogotsi, *Adv. Electron. Mater.*, 2016, **2**, 1600050.

21 B. Xiao, Y.-c. Li, X.-f. Yu and J.-b. Cheng, *Sens. Actuators, B*, 2016, **235**, 103–109.

22 H. Kim, B. Anasori, Y. Gogotsi and H. N. Alshareef, *Chem. Mater.*, 2017, **29**, 6472–6479.

23 H. Lin, S. Gao, C. Dai, Y. Chen and J. Shi, *J. Am. Chem. Soc.*, 2017, **139**(45), 16235–16247.

24 I. Shein and A. Ivanovskii, *Comput. Mater. Sci.*, 2012, **65**, 104–114.

25 Q. Tang, Z. Zhou and P. Shen, *J. Am. Chem. Soc.*, 2012, **134**(40), 16909–16916.

26 M. Khazaei, M. Arai, T. Sasaki, C. Y. Chung, N. S. Venkataramanan, M. Estili, Y. Sakka and Y. Kawazoe, *Adv. Funct. Mater.*, 2012, **23**, 2185–2192.

27 A. Enyashin and A. Ivanovskii, *J. Solid State Chem.*, 2013, **207**, 42–48.

28 I. R. Shein and A. L. Ivanovskii, *Superlattices Microstruct.*, 2012, **52**, 147–157.

29 J. Halim, M. R. Lukatskaya, K. M. Cook, J. Lu, C. R. Smith, L.-Å. Näslund, S. J. May, L. Hultman, Y. Gogotsi, P. Eklund and M. W. Barsoum, *Chem. Mater.*, 2014, **26**, 2374–2381.

30 L. H. Karlsson, J. Birch, J. Halim, M. W. Barsoum and P. O. Persson, *Nano Lett.*, 2015, **15**, 4955–4960.

31 M. R. Lukatskaya, S. M. Bak, X. Yu, X. Q. Yang, M. W. Barsoum and Y. Gogotsi, *Adv. Energy Mater.*, 2015, **5**, 1500589.

32 C. Shi, M. Beidaghi, M. Naguib, O. Mashtalir, Y. Gogotsi and S. J. Billinge, *Phys. Rev. Lett.*, 2014, **112**, 125501.

33 M. Ghidiu, M. Naguib, C. Shi, O. Mashtalir, L. Pan, B. Zhang, J. Yang, Y. Gogotsi, S. J. L. Billinge and M. W. Barsoum, *Chem. Commun.*, 2014, **50**, 9517–9520.

34 B. Anasori, C. Shi, E. J. Moon, Y. Xie, C. A. Voigt, P. R. Kent, S. J. May, S. J. Billinge, M. W. Barsoum and Y. Gogotsi, *Nanoscale Horiz.*, 2016, **1**, 227–234.

35 H.-W. Wang, M. Naguib, K. Page, D. J. Wesolowski and Y. Gogotsi, *Chem. Mater.*, 2015, **28**, 349–359.

36 I. Persson, L.-Å. Näslund, J. Halim, M. W. Barsoum, V. Darakchieva, J. Palisaitis, J. Rosen and P. O. Å. Persson, *2D Mater.*, 2017, **5**, 015002.

37 Y. Dall'Agnese, M. R. Lukatskaya, K. M. Cook, P.-L. Taberna, Y. Gogotsi and P. Simon, *Electrochem. Commun.*, 2014, **48**, 118–122.

38 H. Wang, Y. Wu, J. Zhang, G. Li, H. Huang, X. Zhang and Q. Jiang, *Mater. Lett.*, 2015, **160**, 537–540.

39 T. Li, L. Yao, Q. Liu, J. Gu, R. Luo, J. Li, X. Yan, W. Wang, P. Liu and B. Chen, *Angew. Chem., Int. Ed.*, 2018, **57**, 6115–6119.

40 O. Wilhelmsson, J.-P. Palmquist, E. Lewin, J. Emmerlich, P. Eklund, P. Persson, H. Högberg, S. Li, R. Ahuja and O. Eriksson, *J. Cryst. Growth*, 2006, **291**, 290–300.

41 P. Eklund, M. Beckers, J. Frodelius, H. Högberg and L. Hultman, *J. Vac. Sci. Technol., A*, 2007, **25**, 1381–1388.

42 J. Palisaitis, I. Persson, J. Halim, J. Rosén and P. O. Persson, *Nanoscale*, 2018, **10**, 10850–10855.

43 F. M. Römer, U. Wiedwald, T. Strusch, J. Halim, E. Mayerberger, M. W. Barsoum and M. Farle, *RSC Adv.*, 2017, **7**, 13097–13103.